JOURNAL OF Materials CHEMISTRY

Synthesis of $Li_{1.33}Mn_{1.67}O_4$ spinels with different morphologies and their ion adsorptivities after delithiation

Xiaojing Yang,*[a] Hirofumi Kanoh,[a] Weiping Tang[b] and Kenta Ooi*[a]

[a]*Shikoku National Industrial Research Institute, 2217-14 Hayashi-cho, Takamatsu-shi 761-0395, Japan. E-mail: yang@sniri.go.jp*
[b]*Research Institute for Solvothermal Technology, 2217-43 Hayashi-cho, Takamatsu-shi 761-0301, Japan*

Received 11th January 2000, Accepted 4th May 2000
Published on the Web 29th June 2000

From different precursors, including γ-, β-MnO_2, hollandite, and H^+-form birnessite manganese oxides, well-crystallized $Li_{1.33}Mn_{1.67}O_4$ spinels were synthesized at 400 °C by using $LiNO_3$ as a flux. Alkali metal ion adsorptivities of the spinels after delithiation were investigated. SEM observation showed that each spinel obtained preserved the morphology of its precursor. The lack of morphology change, and the time-dependence of the lithium insertion into the precursors, illustrate that the formation of the spinel is a topotactic template reaction. None of the delithiated spinels preserved the original ion-exchange sites in their precursors but all showed nearly the same high affinity for Li^+, while the amount of uniform acidic sites increased and the steric hindrance during lithiation decreased in the order of spinels obtained from birnessite, hollandite, and γ-, β-MnO_2. This is probably because birnessite has more (buffer) space for the accommodation of ions in its layered structure than other precursors with a tunnel structure and some part of the space remains after structural transformation to the spinel.

1 Introduction

Lithium manganates can be used as electrodes for rechargeable lithium batteries,[1–3] catalysts[4,5] and selective adsorbents.[6,7] Among the family of materials used for the adsorption of Li^+ ions, the protonated form of $Li_{1.33}Mn_{1.67}O_4$ or (Li)[$Li_{0.33}Mn^{IV}_{1.67}$]O_4 spinel has the best selectivity and adsorptivity (around 20 mg g^{-1} Li^+ adsorbed from seawater).[8,9] To synthesize this kind of spinel, a solid-state reaction method is in common use,[10–12] in which an atmosphere of oxygen is needed in order to obtain the tetravalent manganese alone. Takada *et al.*[13] have developed a sol–gel method to prepare well-crystallized $Li_{1.33}Mn_{1.67}O_4$ spinel by heating a eutectic mixture of LiOAc and $Mn(NO_3)_2$ at 700 °C under an O_2 atmosphere.

Inorganic materials with different morphologies can exhibit different properties.[14,15] It could reasonably be supposed that, as one of the properties of selective adsorbents, the adsorption speed would change with the ion path, as shown in Fig. 1; the ion path being controlled by the shape, size, and crystal orientation of adsorbent particles. However, when using the synthesis methods mentioned above, it is difficult to manipulate the crystal particle morphology and, therefore, the ion path.

We have reported[16] that in a $LiNO_3$ flux, $Li_{1.33}Mn_{1.67}O_4$ can be obtained at a low temperature, *e.g.* 400 °C, through the lithiation of β-MnO_2, which comes from the decomposition of the raw material, γ-MnOOH. Although the lithiation reaction causes a structural change from the main phase of β-MnO_2 into $Li_{1.33}Mn_{1.67}O_4$ spinel, it preserves the needle-shaped morphology of β-MnO_2 or γ-MnOOH. This finding provides an approach to the synthesis of $Li_{1.33}Mn_{1.67}O_4$ spinel with controlled crystal shape.

The purpose of this study was to determine whether the synthesis method could be applied to other Mn-resources with different shapes and structures, and also to characterize the obtained materials by ion-exchange capacity and ion-adsorption site measurement. Various Mn-resource raw materials, including β- and γ-MnO_2 with (1 × 1) and (2 × 1) tunnels, hollandite with (2 × 2) tunnels, and birnessite with a (2 × ∞) layer structure were selected. The particle shapes of these precursors are spherical, layered and needle-like, respectively.

2 Experimental

2.1 Synthesis of $Li_{1.33}Mn_{1.67}O_4$ spinels

γ- and β-MnO_2. The MnO_2 reagent used, obtained from High Purity Chemicals Laboratory, Japan, consists of β-MnO_2 and a significant amount of γ-MnO_2 according to its X-ray

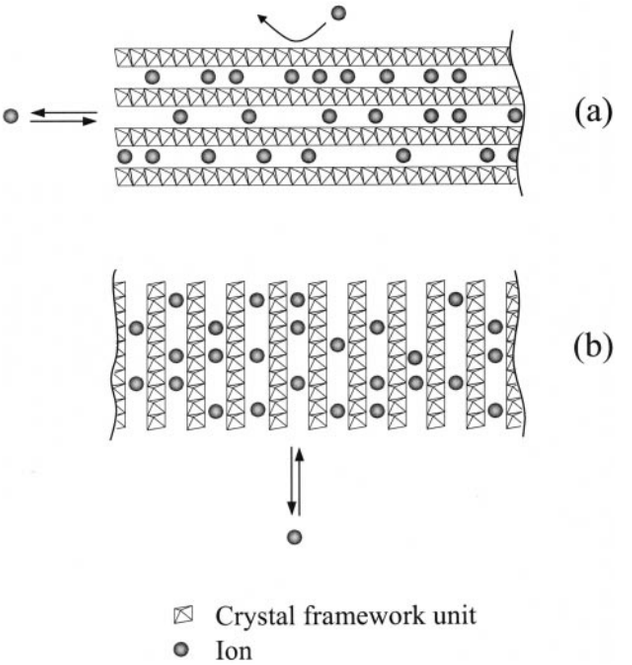

Fig. 1 Schematic diagram of the ion path in different crystal orientations: (a) difficult and (b) easy adsorption/desorption.

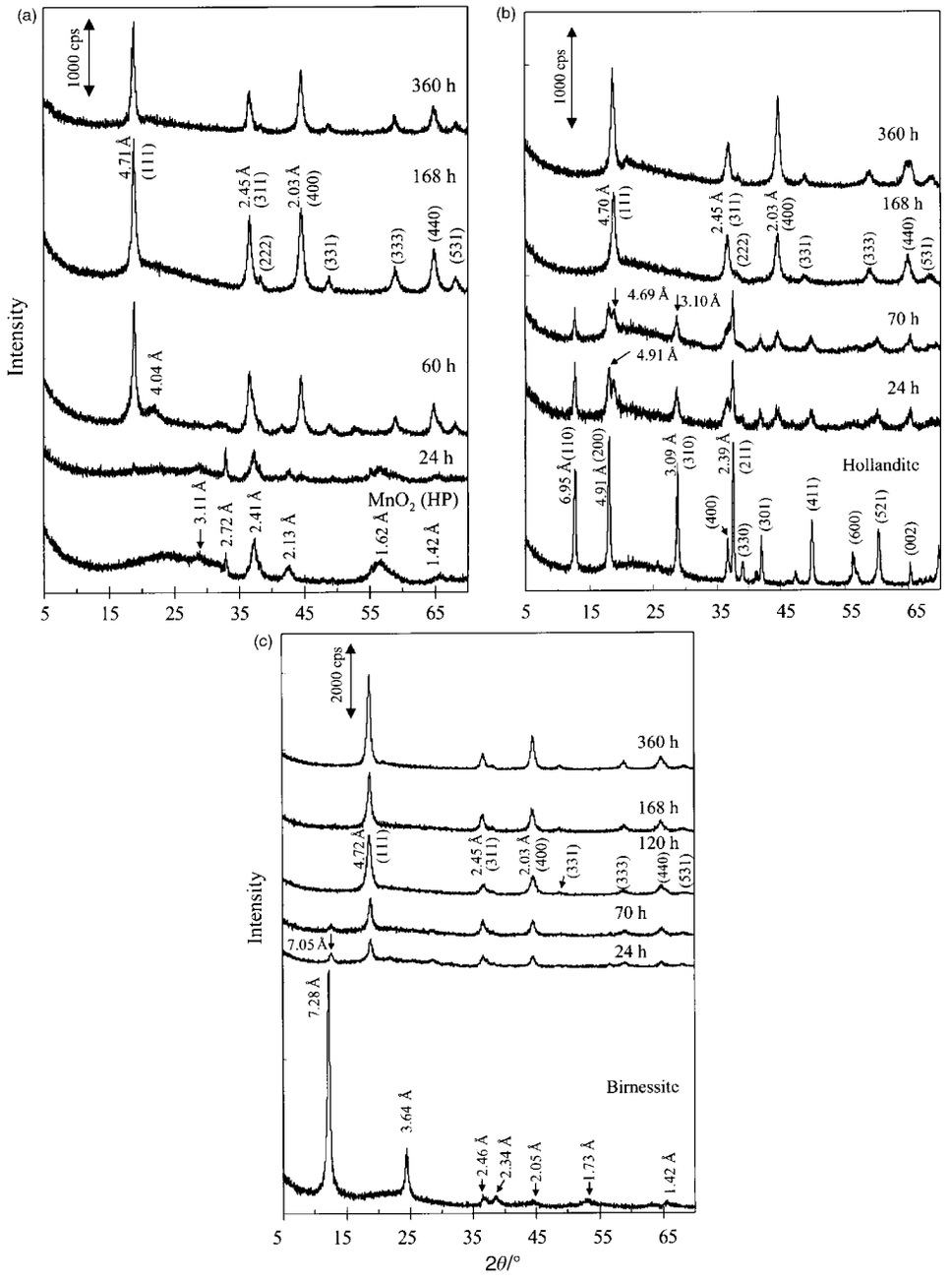

Fig. 2 XRD patterns of the products obtained from the precursors (a) MnO_2 (HP), (b) hollandite and (c) birnessite heated in an $LiNO_3$ flux at 400 °C for different intervals of time.

diffraction pattern (JCPDS card No. 24-735, 12-141, and 30-820), as shown at the bottom of Fig. 2(a). The needle-shaped γ-MnOOH was obtained from Toyo Soda Manufacturing Co. Ltd, as reported previously.[16] It decomposes to a mixture with a main phase of β-MnO_2 and a minor phase of γ-MnO_2 (whose peak appears at $2\theta \approx 22°$ in its XRD pattern), when heated at 400 °C in a $LiNO_3$ flux.[16] These two precursors are hereafter referred to MnO_2 (HP) and γ-MnOOH.

Hollandite. A hollandite-type manganese oxide was obtained by a modification of the method reported by Rossouw *et al.*[17] Li_2MnO_3 (5 g), which was obtained by solid-phase reaction, was hydrothermally treated in 100 ml 3 M H_2SO_4 solution at 90 °C for 3 days. The product was filtered, washed with distilled water, and air-dried at 70 °C.

Birnessite. Na^+-form birnessite was prepared by pouring a mixed solution of 1 M H_2O_2 and 0.5 M NaOH into a solution of 0.3 M $Mn(NO_3)_2$ followed by stirring. The precipitate was filtered and washed with distilled water, and hydrothermally treated in a 2 M NaOH solution at 150 °C for 16 h to improve the crystallinity of this form of birnessite.[18] From the Na^+-form birnessite, H^+-form birnessite was prepared by extracting Na^+ with 0.1 M HCl for 3 days. The Na^+ extraction degree was determined by chemical analysis as 97%. The formula of H^+-form birnessite is shown in Table 1, where the residual Na^+ was neglected. This formula corresponds to that of $Na_4Mn_{14}O_{27}\cdot 9H_2O$ in JCPDS card 23-1046. This raw material is abbreviated as birnessite.

Reagent grade $LiNO_3$ was obtained from Wako Pure Chemical Industries, Ltd. (Japan). $LiNO_3$ was mixed with 1 g of the precursor obtained above, maintaining the molar ratio at Li : Mn = 1 : 17–20. The mixture was put into a pure alumina crucible (50 ml), heated in a muffle furnace at 400 °C for different lengths of time and then air-cooled to room temperature. The products were washed with distilled water three times, filtered and dried at 70 °C.

Table 1 Compositions of synthesized precursors and spinels

	Analyzed formula[a]	Structural feature[b]
Precursor		
Birnessite	$Mn_{14}O_{26.7}\cdot 11.8H_2O$	Basal spacing 7.28 Å
Hollandite	$MnO_{1.97}\cdot 0.56H_2O$	$a_0=b_0=9.77$ Å
		$c_0=2.85$ Å
Spinels from		
Birnessite 120 h	$Li_{1.33}Mn_{1.62}O_4$	$a_0=8.12$ Å
Hollandite 168 h	$Li_{1.36}Mn_{1.69}O_4$	$a_0=8.12$ Å
MnO_2 (HP) 168h	$Li_{1.29}Mn_{1.64}O_4$	$a_0=8.12$ Å
γ-MnOOH 168h	$Li_{1.38}Mn_{1.69}O_4$	$a_0=8.12$ Å

[a]The amount of crystal water was measured by thermal gravimetric analysis. [b]Obtained from XRD peaks in the range $2\theta=5$–$70°$. For all the spinels, average values calculated from the crystal planes (400) and (311). Lattice constant errors were not larger than 0.01 Å.

2.2 Physical analysis

X-Ray diffraction. The precursors and their products were subjected to X-ray diffraction (XRD) on a Rigaku RINT 1200 powder diffractometer with Cu-Kα radiation. The observation was performed at 30 °C and 2θ ranged between 5 and 70°.

Scanning electron microscopy. Morphological observations were performed in a JEOL type JSM-5310 and a Hitachi type S-246N scanning electromicroscope (SEM).

2.3 Chemical analysis

The lithium and manganese contents in the samples were determined by atomic absorption spectrophotometry after being dissolved in a mixed solution of HCl and hydrogen peroxide. The formulae of some samples were calculated by combining these results with an available oxygen analysis carried out by the standard oxalic acid method.[19]

Ion-exchange capacity. Proton form samples were prepared by extraction of Li^+ ions from Li^+-form samples in a solution of 0.5 M HCl for 3 days with stirring. The uptake of alkali metal ions from a mixed solution of 0.1 M MCl and 0.1 M MOH (M = Li, Na, K and Cs) was carried out by shaking 50 mg of the sample in a 5 ml solution for 7 days at room temperature. The alkali metal ion concentration in the supernatant was determined by titration with 0.1 M HCl.

pH titration curve. A 40 mg portion of each protonated form sample was immersed in a mixed solution (4 ml) of 0.1 M MCl + MOH (M = Li, Na, K, Cs) in varying ratios with intermittent shaking at room temperature. After the sample was shaken for 7 days,[8] the pH of the supernatant solution was determined with a Horiba Model M-13 pH meter. Based on the model of ion-exchange reaction shown in eqn. (1);

$$\overline{H^+}+M^+\rightleftharpoons\overline{M^+}+H^+ \quad (1)$$

where bar refers to the species in the solid phase and M^+ to alkali metal ions, the thermodynamic equilibrium constant, K, of the reaction can be defined as eqn. (2);

$$K=\frac{a_H(\overline{f_M}\overline{X_M})}{a_M(\overline{f_H}\overline{X_H})}=K_c(\overline{f_M}/\overline{f_H}) \quad (2)$$

where a is the activity of the cation in solution, $\bar{f}$ the activity coefficient of cations in the solid phase, and $\overline{X}$ the equivalent fraction of species in the solid phase. $K_c=(a_H\overline{X_M})/(a_M\overline{X_H})$ is the selectivity coefficient including the activity coefficient of the metal ions in solution, and can be evaluated from the pH titration data by eqn. (3);[20,21]

$$pK_c=pH-\log[\overline{X_M}/(1-\overline{X_M})]+\log\ a_M\cong pH-\log[\alpha/(1-\alpha)]+\log\ C_M \quad (3)$$

where C_M is the concentration term of metal ions (here $C_M=0.1$) and α is the degree of neutralization. The K value and standard Gibbs energy change (ΔG^0) can be evaluated as eqn. (4) by use of the Gaines–Thomas equation, assuming the change of water content in the exchanger and the entrance of anions from the solution phase can be neglected;[22]

$$\Delta G^0=(2.303RT)pK \quad (4)$$

where

$$pK=-\log\ K=\int_0^1 pK_c\ d\alpha$$

3 Results and discussion

3.1 Li^+-insertion into precursors and morphology of $Li_{1.33}Mn_{1.67}O_4$

The XRD patterns of the products after heating each precursor in a $LiNO_3$ flux at 400 °C for different lengths of time are shown in Fig. 2. With increasing treatment time, the peaks of the precursors decreased and the peaks of $Li_{1.33}Mn_{1.67}O_4$ increased. The peaks of the precursors cannot be observed when the heating time is longer than 168 h (120 h for

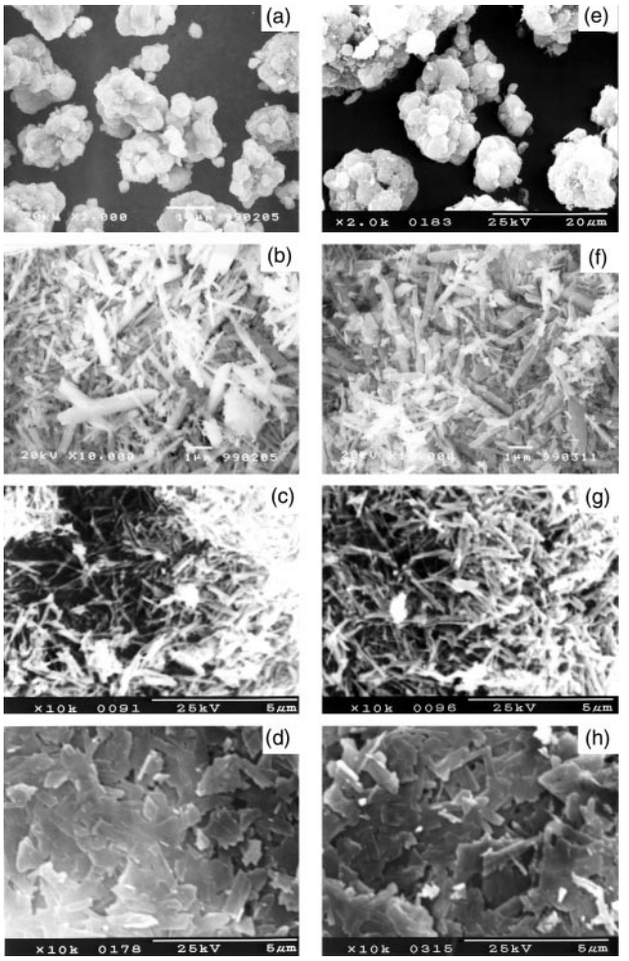

Fig. 3 SEM micrographs of precursors (a) MnO_2 (HP), (b) γ-MnOOH, (c) hollandite, and (d) birnessite, and of their corresponding products (e)–(h) after heating in $LiNO_3$ flux at 400 °C for (e)–(g) 168 and (h) 120 h, respectively.

birnessite). After heating for an even longer time, *e.g.* 360 h, a small peak near the highest peak of spinel emerged, which can be identified as monoclinic Li_2MnO_3. Micrographs of the samples heated for 168 h (120 h for the sample from birnessite) are shown in Fig. 3. Compared with their respective precursors, at least to the extent we can determine with SEM, there were no morphological changes in any products of the spinel crystals. Therefore, the XRD and SEM results demonstrate that the precursors react topotactically with $LiNO_3$ and are converted directly to the $Li_{1.33}Mn_{1.67}O_4$ spinel phase without any other phase appearing during this transition. Monoclinic Li_2MnO_3 could be observed as a result of long-term heating.

The chemically analyzed Li/Mn molar ratios for these samples in Fig. 2 are given in Fig. 4. As shown, Li/Mn ratios increased with heating time. For the precursors MnO_2 (HP), γ-MnOOH and hollandite heated for 168 h and birnessite for 120 h, Li/Mn ratios were around 0.8, the theoretical value of spinel $Li_{1.33}Mn_{1.67}O_4$, coinciding with the spinel peaks in the XRD patterns (Fig. 2). The compositions of these spinels obtained are given in Table 1. Manganese was in the tetravalent state in all the spinels. The Li/Mn curve of the products from MnO_2 (HP) increased smoothly, but in samples obtained from hollandite, the Li/Mn ratio was almost unchanged from 24 to 70 h (Fig. 4). This is most likely because the lithiation of hollandite is easier than for MnO_2 (HP) in aqueous solution (further discussion below). More lithium ions were inserted into birnessite than into other precursors, because the insertion into its layered structure is easier than into a tunnel structure. Therefore, a shorter time is needed for the Li/Mn ratio to reach 0.8 in samples from birnessite than in those from other precursors.

Direct evidence of the lithium insertion into birnessite was shown by the peaks of the XRD pattern in Fig. 2(c). No other new peaks corresponding to other substances appeared. The *d*-value of the peak at $2\theta = 12^\circ$ shifted from 7.28 Å for H^+-form birnessite to 7.05 Å for the samples heated for 24 and 70 h. This means that birnessite did not decompose in the flux at 400 °C and the H/Li ion exchange caused the basal spacing of birnessite to decrease to 7.05 Å. The ion exchange can be written as eqn. (5);

$$H_4Mn_{14}O_{27} + 4Li^+ \rightarrow Li_4Mn_{14}O_{27} + 4H^+ \quad (5)$$

but in Fig. 2(b), the peaks of hollandite did not shift after heating for 24 and 70 h due to the rigid framework of hollandite. The transformation from a precursor to the spinel can be explained in two steps: the first step is the lithium insertion into the precursor and the second step, consequently, formation of the spinel. The reaction for formation of the spinel can be written as eqn. (6) for Li^+-form birnessite obtained from the eqn. (5) reaction, and as eqn. (7) for MnO_2;

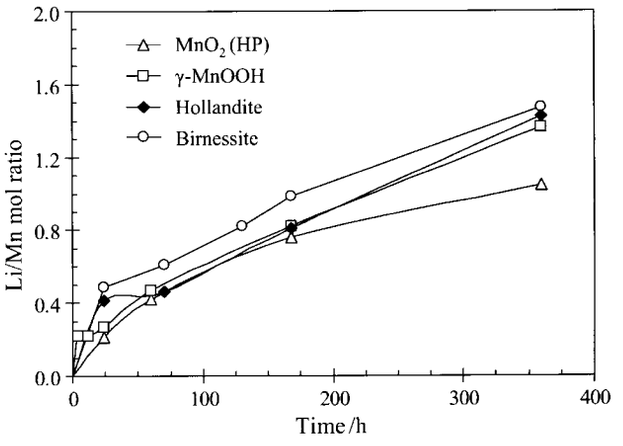

Fig. 4 Relationship between Li/Mn molar ratio in the products and heating time.

$$5Li_4Mn_{14}O_{27} + 36LiNO_3 \xrightarrow{400\,^\circ C} 14Li_4Mn_5O_{12} + 36NO_2 + 3/2O_2 \quad (6)$$

$$5MnO_2 + 4LiNO_3 \xrightarrow{400\,^\circ C} Li_4Mn_5O_{12} + 4NO_2 + O_2 \quad (7)$$

where the crystal water in birnessite and hollandite was not included, because DTA-TG results showed the crystal water vaporized below 400 °C.

According to eqn. (7), 0.4 mol of oxygen ions combined into 1 mol of MnO_2 to form $Li_{1.33}Mn_{1.67}O_4$, accompanying lithiation. That means that the re-adjustment of the framework of $Li_{1.33}Mn_{1.67}O_4$ spinel from MnO_2 is achieved *via* an oxygen-diffusion transition, and in the product the volume of oxygen ions increases by 20% compared with MnO_2. From eqn. (6), the volume of oxygen ions increases by 24.44% compared with the birnessite precursor.

In the spinel of $LiMn_2O_4$, the cubic-close-packed oxide ions occupy positions 32e of space group *Fd*3*m*, and the manganese ions occupy half of the octahedral sites designated 16d, while in the spinel of $Li_{1.33}Mn_{1.67}O_4$, one sixth of the sites that were occupied by manganese ions (16d) in $LiMn_2O_4$ are now occupied by lithium ions.[23] According to David *et al.*,[24] the $[Mn_2]O_4$ framework of the $LiMn_2O_4$ spinel phase is directly accessible from the rutile structure of β-MnO_2 *via* an essentially diffusionless transition. In the present study, however, the transition from MnO_2 and birnessite to $Li_{1.33}Mn_{1.67}O_4$ involves an oxygen-diffusion transition. Two possibilities are considered to explain why the non-morphologic change was observed in Fig. 3. (1) In the precursors, there is a "buffer space" that could be filled up by oxygen ions. The buffer space may counteract the increase of oxygen volume to such an extent that the shape of the precursors is morphologically preserved. In hollandite, the buffer space may be (2×2) tunnels, which allow K^+ ions (radius 1.33 Å) to be inserted, and hence, O^{2-} ions (1.40 Å) can be stored, while in birnessite the buffer space may be the interlayer. Considering the model of David *et al.*, we believe that β-MnO_2 does not possess this buffer space, but that MnO_2 (HP) does, mainly in the form of extensive defects and vacancies that gave rise to XRD line broadening [Fig. 2(a)], together with some (2×1) tunnels of γ-MnO_2. In γ-MnOOH, the buffer space may be the space remaining after the vaporization of H_2O during the decomposition of MnOOH.[16] (2) Alternatively, a portion of the manganese dissolves into the flux, resulting in a diffusionless transition as suggested by the model of David *et al.* However we consider the buffer space explanation to be more likely, when applying it to explain the absorptive behavior of these spinels.

From the discussion above, it can be concluded that the reaction of the precursor with $LiNO_3$ proceeds *via* a topotactic template reaction to form the spinel. Further studies, *e.g.* TEM observation and the use of a pure β-MnO_2 reagent, are needed to explain the relationship between the morphology and framework change and, furthermore, the ion path.

3.2 Adsorptivity for alkali metal ions

Chemical analysis showed that, after acid treatment, almost all of the lithium ions (100, 89, 93 and 96%) were removed from the spinels obtained from MnO_2 (HP), γ-MnOOH and hollandite heated for 168 h and birnessite heated for 120 h, respectively. Ion-exchange capacities of the precursors and their products after delithiation are given in Table 2. MnO_2 (HP) and γ-MnOOH barely took up the alkali metal ions in the aqueous solutions. The spinels obtained from different precursors showed similar ion-exchange capacities, large uptakes of Li^+ and Na^+ ions, and small uptakes of K^+ and Cs^+ ions. The high K^+ uptake capacity in birnessite and hollandite disappeared after their transition to spinel structure.

Fig. 5 illustrates the pH titration curves for alkali metals.

Table 2 Ion-exchange capacities of the precursors and spinels

	Ion-exchange capacity/mmol g^{-1}			
	Li^+	Na^+	K^+	Cs^+
Precursor				
γ-MnOOH	0.40	0.15	0.20	0.10
MnO_2 (HP)	0.85	0.55	0.40	0.30
Hollandite	2.50	1.69	1.35	0.65
Birnessite	3.87	2.55	2.37	2.68
Spinels from				
γ-MnOOH 168 h	5.28	2.22	0.40	0.30
MnO_2 (HP) 168 h	6.36	3.49	1.00	0.49
Hollandite 168 h	6.16	3.05	0.90	0.50
Birnessite 120 h	6.79	3.64	1.49	0.69

Comparing it with Table 2, it is reasonable to consider that the alkali metal/H^+ ion-exchange reactions in MnO_2 (HP) proceed only at the surface of the particles, as do those for Cs^+ and K^+ in all the spinel particles, as described in ref. 20. The apparent adsorptive capacity increased in the order $Li^+ \gg Na^+$ in all the spinels. This order differs from that in the precursors at pH < 7, $K^+ > Na^+ > Li^+$ in hollandite, and $K^+ > Cs^+ > Na^+ > Li^+$ in birnessite, but is the same as that in birnessite at pH > 7. The affinity order change above pH 7 has been explained[21] as probably due to the large steric effect in large unhydrated cations (K^+, Cs^+) at high pH.

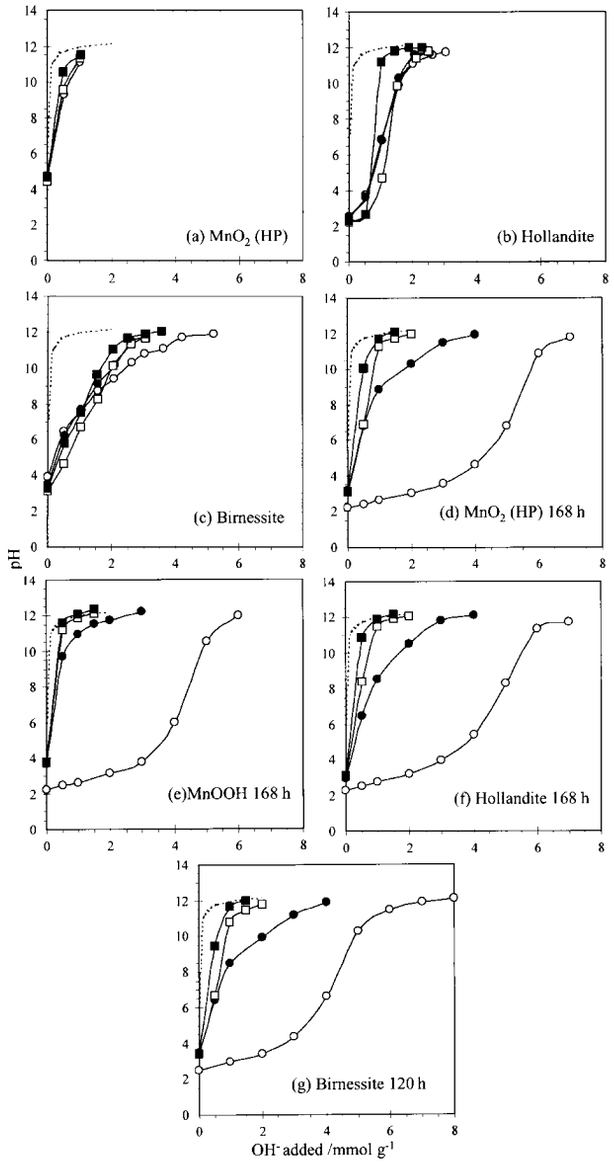

Fig. 5 pH titration curves of the precursors (a)–(c) and the spinels (d)–(g): (○) Li^+, (●) Na^+, (□) K^+, (■) Cs^+; dotted line, blank.

The pK_c value calculated from the data in Fig. 5 against the degree of neutralization, α, is shown in Fig. 6. The intrinsic selectivity coefficient, pK_0, was derived by extrapolating α to zero. Values of pK_0, pK and ΔG^0 are tabulated in Table 3. The spinels from different precursors have nearly the same pK_0 (Li^+/H^+) or pK_0 (Na^+/H^+) values. The value of pK_0, on "zero loading" of the ion-exchange reaction, is a reflection of the action only between the adsorption site and ion. There are three kinds of protons that affect the intrinsic acidity of the adsorption site. (1) A lattice proton, reflected by $pK_0 \approx 2$.[25] The hollandite samples have this kind of site for Li^+, Na^+, and K^+/H^+ ion exchange; the selectivity sequence is $Li^+ < Na^+ < K^+$, as shown in Table 3. The spinels obtained showed that the pK_0 (Li^+/H^+) value was around 2 and they have almost the same affinity for Li^+. (2) A charge-compensating proton, reflected by $pK_0 \approx 4$, which derives from the existence of trivalent manganese. The sites for alkali metal ion/H^+ exchange in birnessite belong to this group, as shown in Table 3. However, the pK_0 (K^+/H^+) value of 3.1 may imply that there are also some lattice proton sites. The selectivity sequence is $Li^+ < Na^+ < Cs^+ < K^+$. (3) A surface proton, $pK_0 \approx 4$.[21] Since manganese ions in the spinels were tetravalent (Table 1), the sites for Na^+/H^+ exchange can be assigned to this group.

Table 3 Values of pK_0, pK and ΔG^0 (temperature 296 K) for the precursors and spinels

Exchanger	Ion	pK_0	pK	$\Delta G^0/10^3$ J mol^{-1}
Precursor				
Birnessite	Li	5.5	8.4	48
	Na	4.6	7.1	40
	K	3.1	6.0	34
	Cs	4.0	7.1	41
Hollandite	Li	2.2	6.5	37
	Na	2.0	5.6	31
	K	1.5	4.3	24
Spinel from				
Birnessite 120 h	Li	2.6	5.5	31
	Na	4.0	7.9	45
Hollandite 168 h	Li	2.4	3.8	21
	Na	3.8	7.8	44
γ-MnOOH 168 h	Li	2.2	3.3	19
	Na	5.0	8.9	50
MnO_2 (HP) 168 h	Li	2.3	3.8	22
	Na	4.3	8.3	47

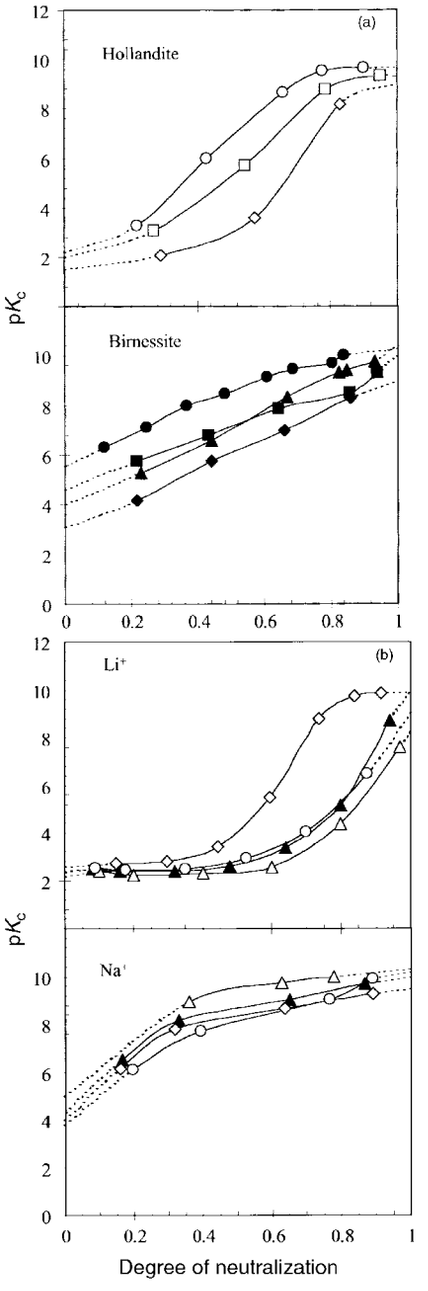

Fig. 6 pK_c *vs.* degree of neutralization plots calculated from Fig. 5. (a) Precursors: hollandite and birnessite. (○, ●) Li^+; (□, ■) Na^+; (◇, ◆) K^+; (▲) Cs^+. (b) Spinels obtained from (△) γ-MnOOH, (▲) MnO_2 (HP), (○) hollandite, and (◇) birnessite.

The ion-sieve effect for K^+ is shown by the selectivity sequence in hollandite and birnessite. After hollandite and birnessite were transformed to spinel form, the adsorption sites for K^+ (and Cs^+) were lost. All the spinels showed stronger affinity for Li^+ than for Na^+. The order of pK_0 (Li^+/H^+) was hollandite ≈ spinels < birnessite.

The hydrated lithium ions exchange with protons in hollandite and birnessite. For this reason, the Li^+/H^+ ion exchange suffers significant steric hindrance, as shown in Fig. 6(a), where the curve of pK_c (Li^+/H^+) rises quickly. The pK_c (Na^+/H^+) and pK_c (K^+/H^+) values also showed a big steric effect, after a slow increase. Although the overall acidity of hollandite is higher than that of birnessite, the existence of Mn^{3+} in birnessite causes its pK_c curves to increase slowly and the free energy ΔG^0 is not as high for each alkali metal ion/H^+ exchange.

The difference in shape of the pK_c curves in spinels from hollandite and birnessite may arise because only non-hydrated lithium ions could exchange with lattice protons in a spinel. ΔG^0 of the spinel from γ-MnOOH was the lowest; therefore, it is lithiated most easily among the spinels obtained. The pK_c *vs.* α curve of the spinel from γ-MnOOH in Fig. 6(b) showed a long unvarying range up to around $\alpha = 0.6$, *i.e.*, it has more uniform acidic sites than do the other spinels. The spinel from birnessite whose curve in Fig. 6(b) went up rapidly from around $\alpha = 0.3$ had fewer acidic sites. This means that the lithiating reaction suffers more steric hindrance than in the other spinels. The uniform acidic site quantity in the spinels increased in the precursor order birnessite, hollandite [MnO_2 (HP)] and γ-MnOOH.

3.3 Relation between adsorptivity and the morphology of the spinel or structure of the precursor

If there were differences in the ion-exchange capacity, a spherical particle would presumably have the highest capacity, because the crystal system of the spinel is cubic. However, the spherical particles [Fig. 3(e)] did not show a higher ion-exchange capacity than other spinel shapes in Fig. 3(f)–(h) (Table 2). So the ion-exchange capacity seems to have nothing to do with the morphology of the spinel.

On the other hand, the order of uniform acidic site quantity corresponds to the precursor's structural space size, *i.e.* interlayer, (2 × 2) [and (2 × 1)] tunnel, and (1 × 1) tunnel. The original adsorption sites for K^+ and Cs^+ in the precursors did not remain in the spinels, while the greater ΔG^0 for Li^+/H^+ corresponds to a lower ΔG^0 for Na^+/H^+ ion exchange. Thus, this uniform acidic site order is probably caused by the difference in the number and distribution of "buffer spaces" remaining in a spinel. After being partly occupied by O^{2-} ions diffusing into the precursor during the formation of the spinel, the buffer space could remain in the spinel. The distribution of the buffer space should depend on the crystal orientations of the precursor and could affect the ion-exchange site distribution in spinel particles.

4 Summary

By heating at 400 °C in an $LiNO_3$ flux, lithium is inserted into H^+-form birnessite with a (2 × ∞) layer structure, hollandite with a (2 × 2) tunnel structure, and γ-, β-MnO_2 with (2 × 1), (1 × 1) tunnels, causing a structural change to $Li_{1.33}Mn_{1.67}O_4$ spinel, while the morphologies of the precursors are preserved at the scale of SEM analysis. Long-term heating results in the insertion of more Li^+ ions, forming Li_2MnO_3.

To form this kind of spinel, oxygen diffusion is necessary. The interlayers and (2 × 2) and (2 × 1) tunnels in the precursors possibly supply some "buffer spaces" for the oxygen ions, and thus no obvious morphology change could be observed.

The pH titration results show that alkali metal/H^+ ion-exchange sites in the precursors disappear after their transition to spinel form. The affinities for Li^+ are nearly the same in all the spinels obtained from different precursors and are much stronger than those for other alkali metal ions. More uniform acidic sites are contained in the spinel obtained from a precursor with relatively smaller pore size (tunnel size). The lithiation of the spinel from birnessite with its layered structure suffers more steric hindrance than that from precursors with a tunnel structure. A possible interpretation of this result is that there are differences in the number and distribution of the "buffer spaces" remaining in exchanger particles.

References

1 A. R. Armstrong and P. G. Bruce, *Nature*, 1996, **381**, 499.
2 M. M. Thackeray, *Prog. Solid State Chem.*, 1997, **25**, 1.

3 A. R. Armstrong, H. Huang, R. A. Jennings and P. G. Bruce, *J. Mater. Chem.*, 1998, **8**, 255.
4 H. Cao and S. L. Suib, *J. Am. Chem. Soc.*, 1994, **116**, 5334.
5 Y. Chabre and J. Pannetier, *Prog. Solid State Chem.*, 1995, **23**, 1.
6 Y. F. Shen, R. P. Zerger, R. N. DeGuzman, S. L. Suib, L. McCuidy, D. I. Potter and C. L. O'Young, *Science*, 1993, **260**, 511.
7 Q. Feng, H. Kanoh, Y. Miyai and K. Ooi, *1995 International Conference on Ion Exchange, Proceedings*, 1995, p. 141.
8 K. Ooi, Y. Miyai and J. Sakakihara, *Langmuir*, 1991, **7**, 1167.
9 Q. Feng, Y. Miyai, H. Kanoh and K. Ooi, *Langmuir*, 1992, **8**, 1861.
10 G. V. Leont'eva and L. G. Chirkova, *J. Appl. Chem., USSR*, 1988, **61**, 660.
11 K. Ooi, Y. Miyai and K. Katoh, *Solvent Extr. Ion Exch.*, 1987, **5**, 561.
12 T. Takada, H. Hayakawa, T. Kumagai and E. Akiba, *J. Solid State Chem.*, 1996, **121**, 79.
13 T. Takada, H. Hayakawa and E. Akiba, *J. Solid State Chem.*, 1995, **115**, 420.
14 J. Hulliger, *Angew. Chem., Int. Ed Engl.*, 1994, **22**, 143.
15 Z. Han, S. Yu, Y. Li, H. Zhao, F. Li, Y. Xie and Y. Qian, *Chem. Mater.*, 1999, **11**, 2302.
16 X. Yang, W. Tang, H. Kanoh and K. Ooi, *J. Mater. Chem.*, 1999, **9**, 2683.
17 M. H. Rossouw, D. C. Liles and M. M. Thackeray, *J. Electrochem. Soc.*, 1998, **145**, 582.
18 Q. Feng, K. Yanagisawa and N. Yamasaki, *J. Porous Mater.*, 1998, **5**, 153.
19 Japan Industrial Standard (JIS), 1969, M8233.
20 K. Ooi, Y. Miyai, S. Katoh, H. Maeda and M. Abe, *Bull. Chem. Soc. Jpn*, 1988, **61**, 407.
21 K. Ooi and M. Abe, *Solvent Extr. Ion Exch.*, 1996, **16**, 1137.
22 G. L. Gaines, Jr. and H. C. Thomas, *J. Chem. Phys.*, 1953, **21**, 714.
23 B. Ammundsen, D. J. Jones and J. Roziere, *Chem. Mater.*, 1998, **10**, 1680.
24 W. I. F. David, M. M. Thackeray, P. G. Bruce and J. B. Goodenough, *Mater. Res. Bull.*, 1984, **19**, 99.
25 Q. Feng, Y. Miyai, H. Kanoh and K. Ooi, *Langmuir*, 1992, **8**, 1861.